

Electron cloud predictions for the Hadron Storage Ring of the Electron-Ion Collider and planned mitigations

S. Verdu-Andres

September 2025

Electron-Ion Collider
Brookhaven National Laboratory

U.S. Department of Energy
USDOE Office of Science (SC), Nuclear Physics (NP)

Notice: This technical note has been authored by employees of Brookhaven Science Associates, LLC under Contract No. DE-SC0012704 with the U.S. Department of Energy. The publisher by accepting the technical note for publication acknowledges that the United States Government retains a non-exclusive, paid-up, irrevocable, world-wide license to publish or reproduce the published form of this technical note, or allow others to do so, for United States Government purposes.

DISCLAIMER

This report was prepared as an account of work sponsored by an agency of the United States Government. Neither the United States Government nor any agency thereof, nor any of their employees, nor any of their contractors, subcontractors, or their employees, makes any warranty, express or implied, or assumes any legal liability or responsibility for the accuracy, completeness, or any third party's use or the results of such use of any information, apparatus, product, or process disclosed, or represents that its use would not infringe privately owned rights. Reference herein to any specific commercial product, process, or service by trade name, trademark, manufacturer, or otherwise, does not necessarily constitute or imply its endorsement, recommendation, or favoring by the United States Government or any agency thereof or its contractors or subcontractors. The views and opinions of authors expressed herein do not necessarily state or reflect those of the United States Government or any agency thereof.

Electron cloud predictions for the Hadron Storage Ring of the Electron-Ion Collider and planned mitigations

Silvia Verdú-Andrés*

Brookhaven National Laboratory, Upton, NY 11973, USA

(EIC Project)

This paper reports on a collection of electron cloud studies to determine the electron cloud threshold for different sections along the beampipe of the Hadron Storage Ring (HSR) for the Electron-Ion Collider (EIC), presents the results of a study of the interaction of the beam with the electron clouds, and discusses the limitation of potential solutions like scrubbing and Landau damping.

I. ELECTRON CLOUDS IN HIGH-INTENSITY POSITIVELY-CHARGED PARTICLE ACCELERATORS

Electron cloud buildup is the avalanche electron multiplication in the vacuum chamber of a particle accelerator which results from the emission of secondary electrons from the walls of the vacuum chamber after the impact of a primary electron and establish resonant trajectories due to coupling with the electromagnetic field generated by the passing beam bunches that extract further electrons. The electron cloud buildup mechanism is analogous to the multipacting effect in RF components. Whereas multipacting is fed by the electromagnetic energy stored in the RF component, in particle accelerators the beam feeds the electron cloud buildup.

Electron clouds have been observed in almost every particle accelerator operating with high-intensity positively-charged beams (positrons, protons, heavy ions) [1, 2]: the Proton Storage Ring (PSR) at Budker Institute of Nuclear Physics (BINP) [3–5]; ZGS at Argonne National Laboratory; the PSR at Los Alamos National Laboratory (LANL) [6–8]; PEP-II in 2000 at SLAC; the Alternating Gradient Synchrotron (AGS) [9] and the Relativistic Heavy Ion Collider (RHIC) at Brookhaven National Laboratory (BNL); Bevatron at Lawrence Berkeley National Laboratory; the Intersecting Storage Rings (ISR), the Proton Synchrotron (PS) [10, 11], the Super Proton Synchrotron (SPS) [12] and the Large Hadron Collider (LHC) [13, 14] at CERN; on SNS in 2006 at Oak Ridge National Laboratory; the DAΦNE electron-positron collider at INFN Frascati in Italy; on PETRA-III at DESY in 2009; ISIS at RAL in 2008; the photon and B factories at KEK; the Cornell Electron Storage Ring (CESR) at Cornell during a dedicated study program with a positron beam; and in the Main injector and the Recycler proton storage ring at Fermilab [15].

Electron clouds can heat up the vacuum chamber [16], deteriorate vacuum [17] and beam quality [16, 18, 19], and in some cases lead to beam loss [16].

II. THE HADRON STORAGE RING

OF THE ELECTRON-ION COLLIDER

The Electron-Ion Collider (EIC) will provide high-luminosity collisions of polarized electrons with polarized protons and light ions as well as with heavier stable nuclei in a center-of-mass energy range from 20 to 140 GeV. A sketch of the EIC accelerator complex is shown in Fig. 1.

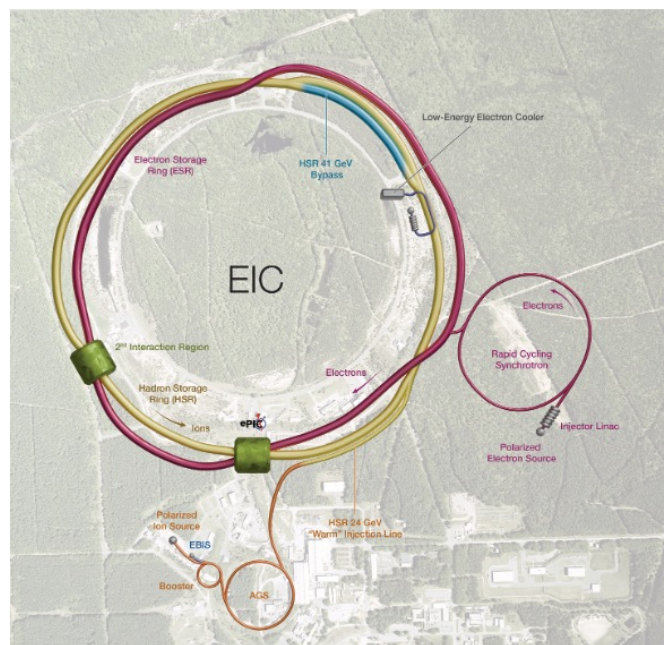


FIG. 1. Sketch of the EIC accelerator complex at BNL.

The Hadron Storage Ring (HSR) of the EIC will host up to 1160 bunches, 1 A beam current of proton and ion beams with an energy range from 40 to 275 GeV. The asymmetric collisions between beams of different species and energies require to adjust the path length of the hadron beams in order to synchronize the collision of hadrons and ultra-relativistic electrons at the interaction point. The path length of the hadron beams is done by a horizontal orbit offset for the 100 and 275 GeV beams and by a by-pass for the 41 GeV beams. Flat beams with a small vertical beam emittance of 1.5 nm are necessary to match the beam size of hadron and electron beams at the interaction point in order to maintain proton beam stability and ensure proton beam lifetime.

* Contact author: sverdu@bnl.gov

The HSR will be built from one of the two superconducting storage rings of the existing Relativistic Heavy Ion Collider (RHIC) of Brookhaven National Laboratory (BNL). In operation since 2001, RHIC has exceeded design luminosity by a factor of 44 and is the world's only polarized proton collider. RHIC can collide up to 110 bunches of diverse ion species ranging from protons to uranium with an energy of up to 255 GeV for proton beams and 100 GeV/n for gold beams.

Electron cloud effects were first observed in RHIC in 2001 [20, 21]. Over the years, several mitigation strategies were adopted [22]. NEG coating in the warm, straight sections suppressed the dynamic pressure surges attributed to electron clouds. Electron clouds still appear during transition crossing with gold beams. The main suspicion is that electron clouds build up in the arc dipoles as the bunch shortens during transition crossing. The superconducting arcs of RHIC have a round, 69 mm diameter, stainless steel 316LN grade beam pipe, which under beam scrubbing can reach a maximum secondary electron yield (SEY) at normal incidence of about 1.35 [23].

On the other hand, LHC has encountered major limitations to operate with 25 ns bunch spacing due to electron clouds. Lengthy scrubbing campaigns to decrease the bunch spacing from 50 to 25 ns and low SEY coatings are planned for HL-LHC. The superconducting arcs of LHC have a beam screen with an inner surface of copper inserted in the bore hole. The main purpose of the LHC beam screens is to shield the dynamic heat load contributed by the beam from the 2 K beam pipe of the superconducting magnets.

The HSR will host proton beams with bunch charge comparable to RHIC and the LHC, and much closely spaced bunches – see Table I. These two beam parameters are believed to be main drivers for electron cloud buildup. Electron clouds have made their appearance in both RHIC and the LHC, which leads us to suspect that electron clouds may also appear in the HSR unless the RHIC beam pipe is upgraded.

TABLE I. Relevant beam parameters of selected high-intensity proton accelerators where electron cloud was observed.

Machine	RHIC	LHC	EIC HSR
Bunch spacing (ns)	108	50 – 25	10.15
Bunch charge ($\times 10^{11}$ ppb)	1.35	1.15	0.69

The studies presented in this paper focus on the proton beam for the highest-luminosity scenario as it is the highest-intensity, shortest bunch spacing beam that the HSR will host, although the beam for the highest center-of-mass scenario is also discussed given its relevance for the commissioning of the machine. Table II lists the main parameter values for both beams. Ramp up from injection energy to store will be performed with the beam circulating on-center of the beam pipe. At store, the

beam orbit aligns with the center of the EIC HSR vacuum chamber. In collision mode, for synchronicity of the electron bunches with ultra-relativistic proton bunches at the interaction point, the 275 GeV proton beams circulate through the arcs with an offset of up to ± 21 mm. The maximum orbit excursion will be at arc quadrupoles and arc sextupoles.

TABLE II. Proton beam parameter values for the highest center-of-mass energy (E_{CM}) and the highest luminosity (\mathcal{L}) beam scenarios.

Parameter	Highest E_{CM}	Highest \mathcal{L}
Species	p^+	p^+
Energy (GeV)	275	275
No. bunches	290	1160
Bunch spacing (ns)	40.59	10.15
Bunch charge (10^{10})	19.1	6.9
RMS bunch length (cm)	6	6
Center-of-Mass Energy (GeV)	140.7	104.9
Luminosity ($10^{33} \text{ cm}^{-2}\text{s}^{-1}$)	1.54	10

III. NUMERICAL PREDICTIONS OF ELECTRON CLOUD BUILDUP THRESHOLDS IN THE HSR

Evaluation of the electron cloud buildup thresholds is essential during the design phase to lay out proper mitigation plans and define design system requirements and specifications. The electron cloud thresholds are set by the heat load budget allocated to the electron cloud contribution to ensure beam quality.

A. Background

The uppermost atomic layers of the vacuum chamber surface will determine the number of secondary electrons emitted (N_s) relative to the number of incident electrons (N_p) at a certain impact energy (E_p) and incidence angle (θ), or secondary electron yield (SEY):

$$SEY(E_p, \theta) = \frac{N_s}{N_p(E_p, \theta)} \quad (1)$$

The SEY of a surface depends on its topography and electronic structure, as well as the presence of absorbates.

B. Method

In this section, the heat load deposited by the electron cloud is used as a monitor to determine the electron cloud buildup threshold. Electron density and heat load are well correlated. The electron cloud buildup threshold, i.e. the SEY value at which the electron cloud initiates

its exponential build up, is identified with the electron density onset. This approach is followed because electron cloud buildup simulations are less computationally expensive than beam - electron cloud interaction simulations. The validity of this approach is later discussed in Section IV.

The electron cloud buildup thresholds are determined by PyECLOUD [24] simulations. The simulations inspect how the electron cloud buildup threshold varies in function of the SEY value (variable "SEY") using the default SEY curve model in the PyECLOUD code ('ECLLOUD') [24, 25], with the model parameters taking the values shown in Table III for amorphous carbon [26].

TABLE III. Parameters from PyECLOUD SEY curve model 'ECLLOUD' and measured values for amorphous carbon [26].

R_0	0.7-0.9
E_0 (eV)	150
E_{\max} (eV)	275.1
s	1.773
δ_{\max} (variable "SEY")	1.06

C. Results

1. Arc dipoles, quadrupoles, and sextupole magnets

The superconducting magnets in the HSR arcs will be equipped with a beam screen. The screen profile adopts the racetrack cross section shown in Fig. 2. In the past, electron cloud thresholds were investigated for round and polygonal profiles [27, 28]. These designs were abandoned with the adoption of the actively-cooled screen as a baseline [29]. Some electron cloud can be tolerated as long as the electron cloud does not compromise beam quality and stability and the heat load from electron cloud does not exceed the about 50–80 W budgeted per sextant.

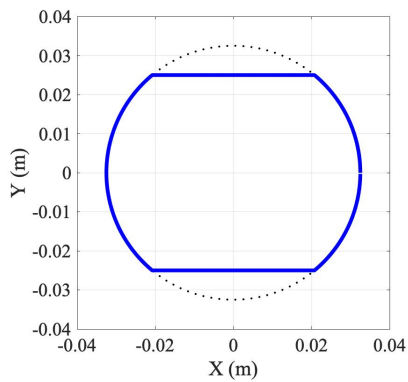


FIG. 2. Racetrack profile of the HSR beam screen.

Fig. 3 shows the heat load deposited by the electron cloud for the highest luminosity and highest Ecm beams

when traveling 18 mm off-center. The highest luminosity beam – with 1160 bunches – shows lower SEY thresholds (around 1.02) than the highest Ecm beam – which contains 290 bunches with larger bunch charge. The screens at the arc quadrupoles show the lowest SEY threshold for the highest Ecm beam while those at the arc sextupoles show the lowest SEY threshold for the highest luminosity beam. The difference in SEY threshold for the focusing and defocusing magnets arises from differences in the magnet strength – see Table V. The lowest SEY threshold for the arc dipoles is found when the highest luminosity beam travels on axis, as shown in Fig. 4. Beam offset scans for the highest luminosity beam and the strongest gradient magnets of each type – the most demanding scenario – are shown in Fig. 5, 6 and 7. The electron cloud buildup response to different beam offsets depends on the magnet type. The known behaviour of higher order magnets as magnetic bottles is enhanced by the beam offset.

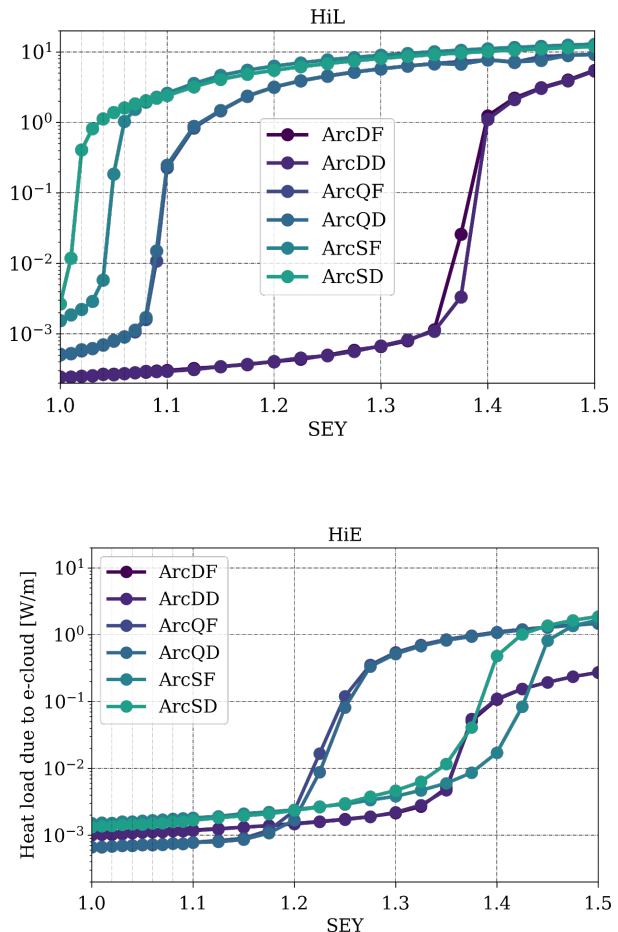


FIG. 3. Heat load due to electron cloud buildup for high-luminosity (top) and highest Ecm (bottom) beams traveling at 18 mm off-center through arc dipoles (DF, DD), arc quadrupoles (QF, QD), and arc sextupoles (SF, SD).

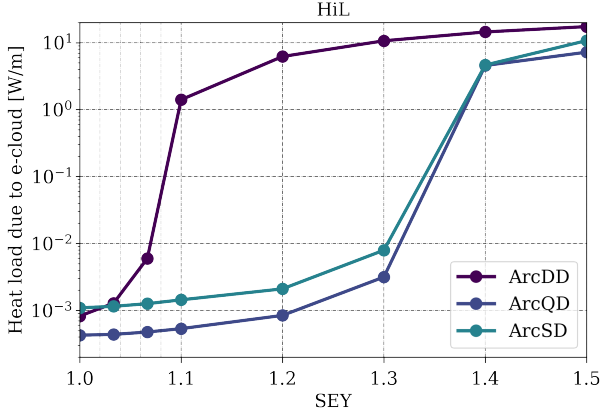


FIG. 4. Heat load due to electron cloud buildup for highest luminosity beam traveling on axis.

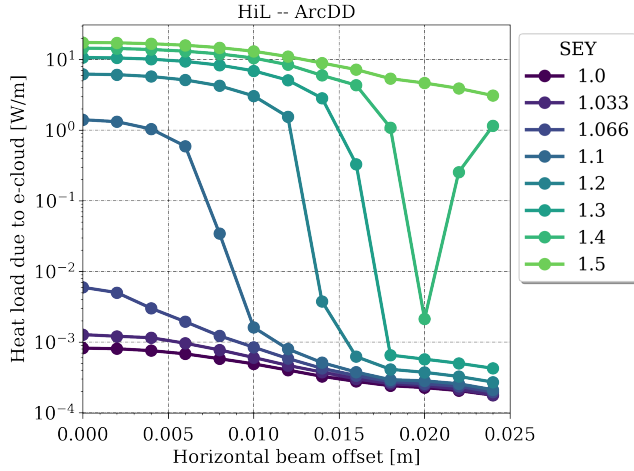


FIG. 5. Heat load due to electron cloud buildup for high luminosity beam in screens of the arc dipole magnets.

A low SEY is required for the vacuum chamber of the HSR superconducting magnets. The baseline plan is to apply a thin layer of amorphous carbon ($\text{SEY} \sim 1$, no need for activation by baking) to the screen. In practice, the produced amorphous carbon films will feature an SEY that follows a bell curve like distribution [30, 31]. Physisorbed molecules on the amorphous carbon surface may also increase the apparent SEY [32]. Table IV lists the heat deposited by the electron cloud for selected SEY values. Scrubbing might be needed during commissioning / pre-operations and there should be some budget allocated to the heat deposited by the scrubbing beam. As the spatial distribution of delivered dose depends as well on the magnet type and beam offset, operation at different beam offsets entails consequences for the scrubbing campaign. Scrubbing beams may be required to clear electron cloud in the superconducting arcs (see Sec-

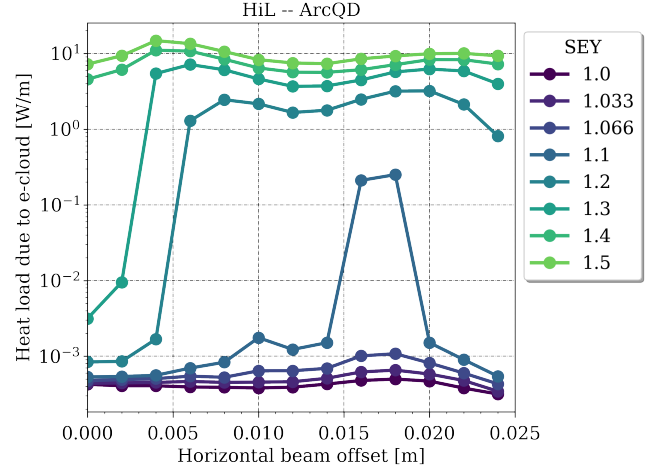


FIG. 6. Heat load due to electron cloud buildup for high luminosity beam in screens of the arc quadrupole defocusing magnets.

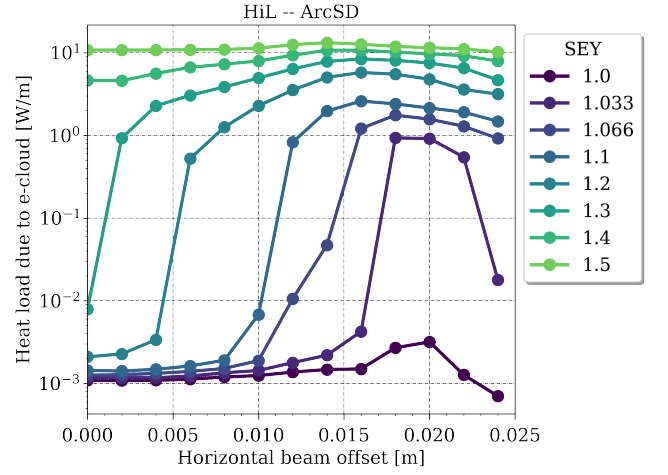


FIG. 7. Heat load due to electron cloud buildup for high luminosity beam in screens of the arc sextupole defocusing magnets.

tion V).

2. Cold mass interconnects

The cold mass interconnects will host new button beam position monitors (BPM) and RF shielded bellows. In presence of no external fields and during operation with colliding (off-centered) beams, Fig. 8 shows that electron cloud will build up in presence of the highest luminosity beam for SEY values featured by conventional metallic surfaces like copper (up to 1.7) and scrubbed stainless steel (1.48).

The beam offset at the cold mass interconnects will vary in a broad range, depending on their location along

TABLE IV. Heat loads (W/m) for selected SEY values of the screens at the magnets (from Fig. 3, 18 mm beam offset) and drifts (from Fig. 8, on-axis beam) of the HSR arcs.

SEY	1.1	1.2	1.3
Highest \mathcal{L}			
Drift	0.0040	3.4362	9.2767
Arc dipole	0.0003	0.0004	0.0007
Arc quadrupole	0.2478	3.1756	5.7655
Arc sextupole	2.4035	5.4965	8.0734
Highest E_{CM}			
Drift	0.0032	0.0037	0.0043
Arc dipole	0.0012	0.0015	0.0022
Arc quadrupole	0.0008	0.0017	0.5161
Arc sextupole	0.0017	0.0023	0.0047

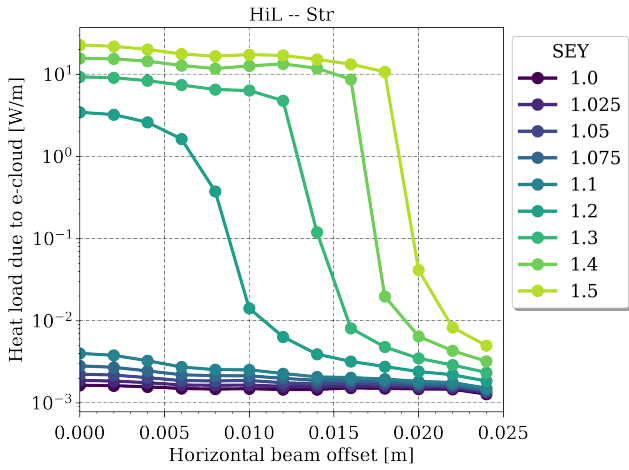


FIG. 8. Heat load due to electron cloud buildup by the highest luminosity beam for no field section with nominal aperture racetrack profile.

the lattice. The lowest SEY threshold is found for the passage of the beam on-axis, as shown in Fig. 9.

The fringe fields of the magnets could make the electron cloud stronger. This result suggests that the surfaces exposed to the beam in the cold mass interconnects must have amorphous carbon coating or any other solution that shows a sufficiently low SEY to prevent electron cloud buildup. The HSR will be warmed up every year, with the fingers of the RF shielded bellows scratching against the edge of the cuff during thermal cycles and risk to flake if coated with amorphous carbon. The coating hardness should be assessed. From Fig. 10, the highest Ecm beam does not seem to build up an electron cloud.

Figures 11 and 12 show the heat deposited by the electron cloud generated by the highest luminosity beam to the screen profile and to the 20-mm diameter BPM button which is farthest away from the beam for different SEY values of the racetrack profile chamber, respectively.

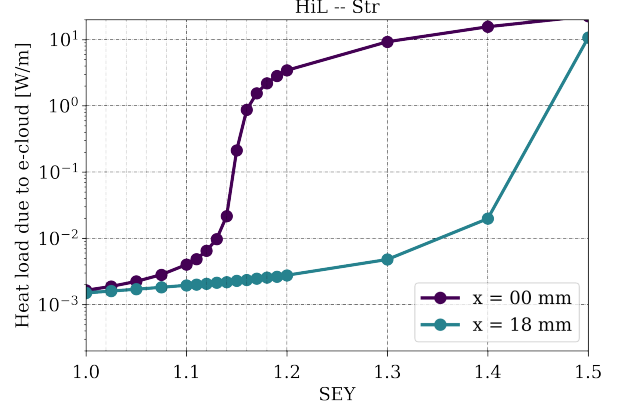


FIG. 9. Heat load due to electron cloud buildup by centered ($x=0$) and off-axis ($x = 18$ mm) highest luminosity beam (top) for no field section with nominal aperture racetrack profile.

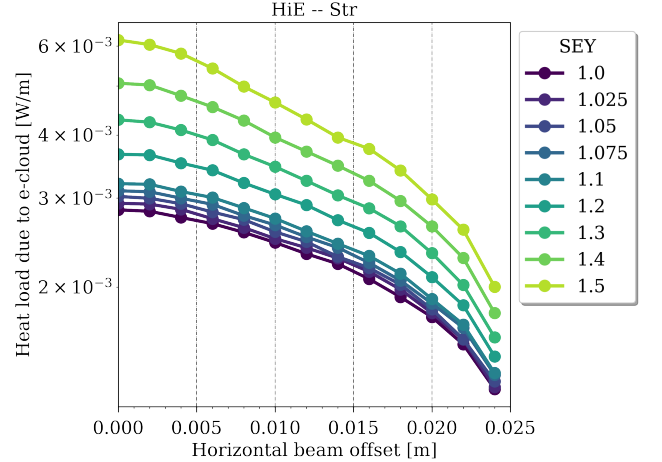


FIG. 10. Heat load due to electron cloud buildup by the highest Ecm beam for no field section with nominal aperture racetrack profile.

3. D0 magnets in IR08

The present HSR design will use warm D0 magnets in all the straight sections. At the time of this study, a lattice solution for the D0s in IR08 was not available, so we assumed a value of 100 m for both beta functions and dispersion not larger than 10 cm, with a nominal field in the D0 of 3.698 T for the 275 GeV proton beam [33]. The D0 beam pipe is 89 mm diameter. Fig. 13 and 14 show the heat load deposited by electron cloud in the D0 magnets of IR08 computed for a 89 mm-diameter round chamber values in case a screen is deemed necessary. The results indicate that some low SEY (< 1.2) surface is needed to suppress electron cloud buildup in this region.

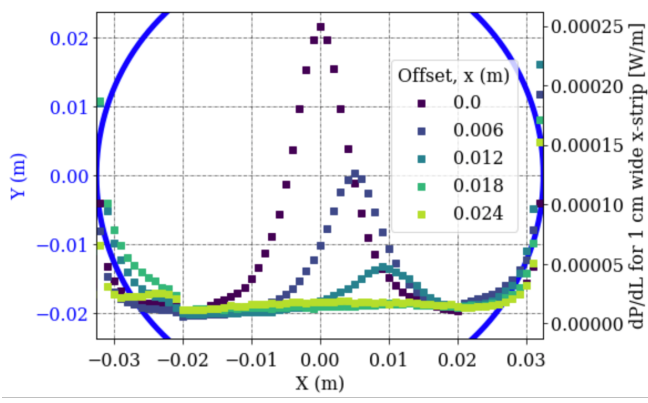


FIG. 11. Heat map along horizontal coordinate X of a nominal aperture racetrack profile with $SEY = 1.1$ due to electron cloud buildup by highest luminosity beam traveling at selected beam offsets x through no field region. The chamber profile is shown in blue.

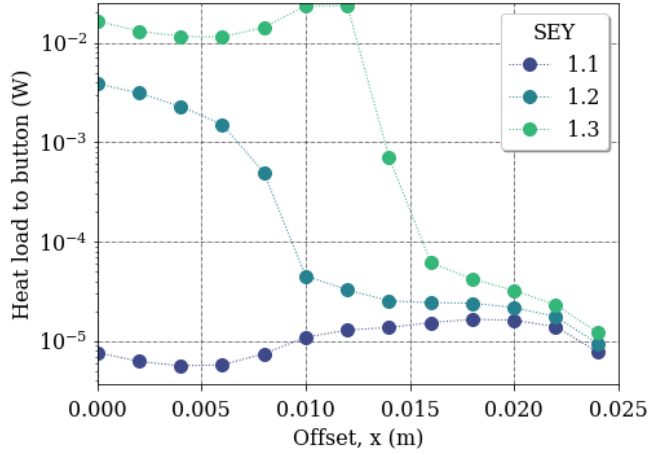


FIG. 12. Heat (W) deposited to a single 20 mm-diameter BPM button located at $x = 26.2$ mm by electron cloud from highest luminosity beam traveling through no-field region in a racetrack profile chamber. Worst case is for button farther away from the beam.

IV. NUMERICAL SIMULATIONS OF BEAM - ELECTRON CLOUD INTERACTION

The following beam-electron cloud interaction studies intend to evaluate the impact of a forming electron cloud on beam stability and, given that the dynamic heat load budget can accommodate some contribution from electron cloud, find the most limiting threshold to electron cloud buildup.

A. Method

The stability studies focus on the 275 GeV highest luminosity proton beam in store (60 mm rms bunch length

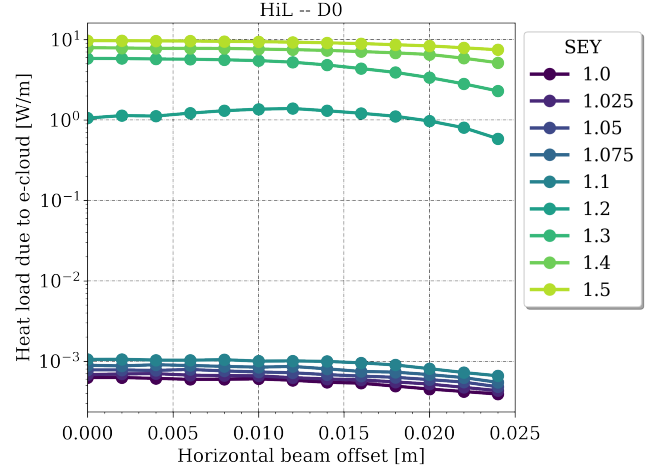


FIG. 13. Heat load due to electron cloud buildup for D0 magnets in IR08 (89 mm-diameter round profile).

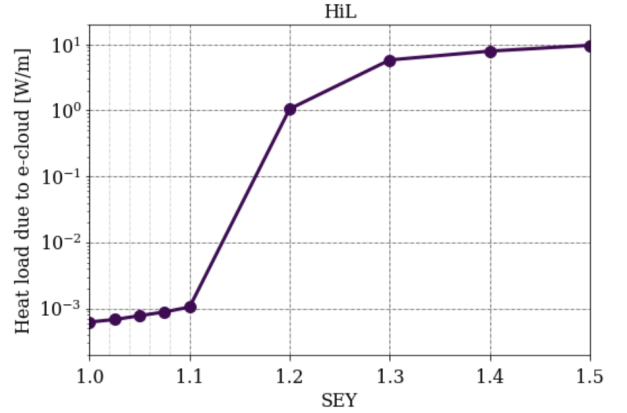


FIG. 14. Heat load due to electron cloud buildup for D0 magnets in IR08 (89 mm-diameter round profile) for centered highest luminosity beam in function of SEY.

beam circulating on-axis). The studies evaluate the interaction of an already formed electron cloud with a bunch at the end of the train tail. For the studied beam, the electron cloud is still forming during the passage of the first few hundred bunches before reaching saturation, as shown in Fig. 15. Following the approach in Ref. [?], the studies assume a uniform distribution of electrons at rest in the vacuum chamber of an arc dipole, corresponding to the electron density of an electron cloud in a saturation regime generated by the last bunches of the train. The assumption of uniform density at beam position is validated from Fig. 16, which shows the electron distribution from a beam traveling on-axis in the vacuum chamber of an HSR arc dipole, right before and after a bunch passage, with the electron cloud in saturation regime. The beam screen surface has $SEY = 1.1$. The electron distribution in the surroundings of the beam right after the bunch passage is uniform. The electron density depends

on the SEY value of the vacuum chamber surface, as shown in Fig. 17. PyECLOUD simulations are used to find the correlation between electron density and SEY value. Stability studies are performed for different electron densities (that is, SEY values). Noting that electron clouds cause fast instabilities, the simulations track for about 10000 turns (about 0.13 seconds) or until 10% of the beam is lost. The electron cloud kick is computed by PyECLOUD and incorporated into PyHEADTAIL [34] as a thin lens element. PyHEADTAIL simulations then track a single bunch around the ring.

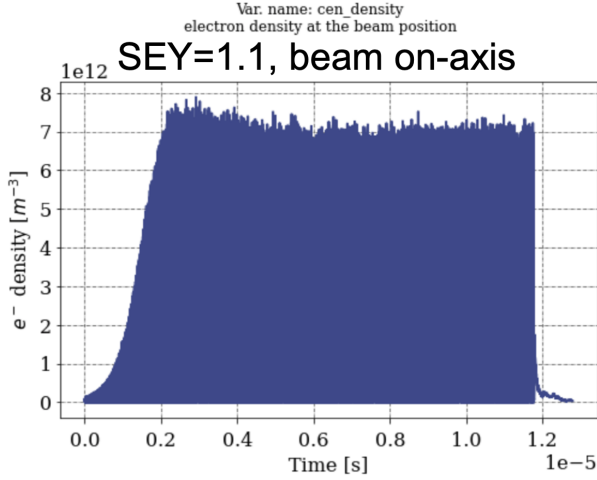


FIG. 15. Electron density at the beam position for a full train of the highest luminosity proton beam.

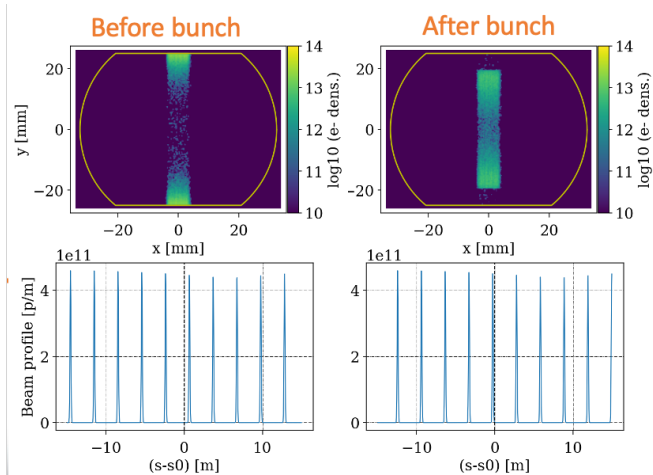


FIG. 16. Electron distribution in the vacuum chamber of an HSR arc dipole, right before and after a bunch passage, with the electron cloud in saturation regime.

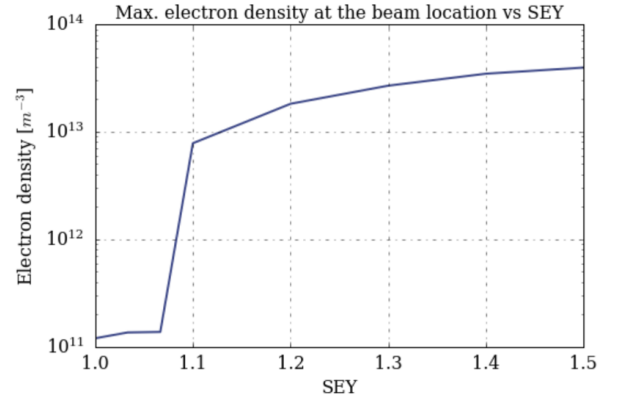


FIG. 17. Electron density is a function of the SEY value of the surface.

B. Results

1. Effects of the interaction on the beam

A stability simulation considering the beam interaction with the electron cloud generated in the beam screen of every HSR arc dipole with SEY = 1.3 surface (electron density of 1×10^{13} electrons/m³ at the beam location) finds that the 10% particle loss limit is reached within few thousand turns. The interaction of the beam with the electron cloud leads to a fast (few tens of milliseconds) vertical emittance blowup, as seen in Fig. 18. An initial bunch centroid wiggling leads to the subsequent vertical emittance blowup, as observed from Fig. 19. The vertical coordinate is more impacted because the electron cloud generated in the field of an arc dipole provides a vertical kick. An inspection of the bunch at the end of the train finds that its interaction with the electron cloud has resulted in a fast growth, transverse head-tail, high-order mode instability, as observed in Fig. 20 for SEY = 1.2.

The previous cases are chosen for illustrative purposes, as the average SEY value for the beam screens of the HSR arc dipoles, coated with amorphous carbon, should present lower SEY values [31]. A study of how the number of dipoles with electron cloud impacts beam stability found that the associated emittance growth will still appear even if the number of arc dipoles with electron clouds is smaller, although the buildup time will be proportional to the number of arc dipoles with electron cloud. Fig. 21 shows that the evolution of the normalized transverse emittance for 100% arc dipoles and 50% arc dipoles with electron clouds overlap after properly weighting number of turns and the total length with electron cloud, indicating that once a certain electron density can trigger the electron cloud instability, the number of turns it takes for the instability to grow is proportional to the length of the region with electron cloud. The case of 10% arc dipoles with electron cloud requires more turns to fully develop the electron cloud instability.

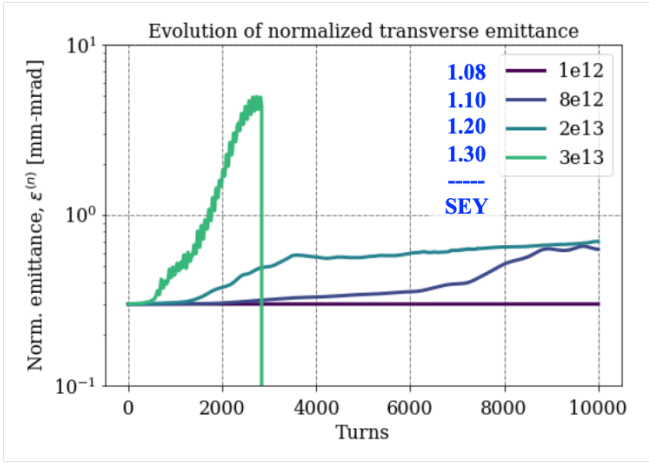


FIG. 18. Evolution of normalized transverse emittance due to interaction with the electron cloud generated by the highest luminosity beam in the vacuum chamber of the HSR arc dipoles with different SEY values.

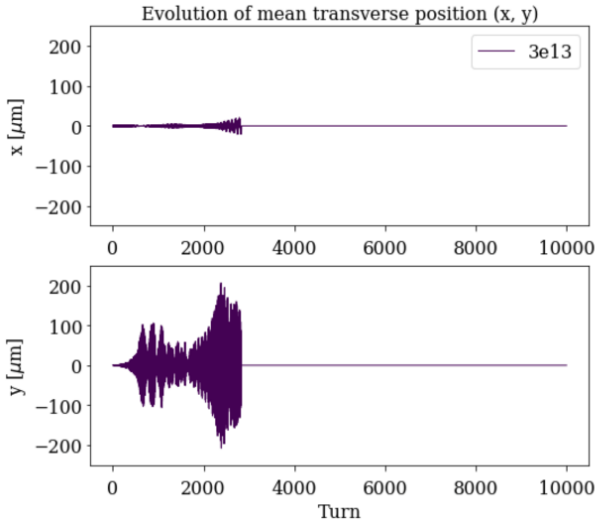


FIG. 19. Motion of the bunch centroid due to interaction with the electron cloud generated by the highest luminosity beam in the vacuum chamber of the HSR arc dipoles with SEY = 1.3.

2. Threshold from beam stability

The dynamic heat budget has margin to accommodate some contribution from electron cloud. This margin can also become handy for beam scrubbing. The electron cloud thresholds are defined to guarantee reliable nominal operations and thus must encompass the dynamic heat load limitations as well as the effects that the interaction of beam and electron cloud have on beam quality and stability.

The stability study is repeated for different values of electron density at the beam location. The results showed in Fig. 18 suggest an alarmingly fast electron

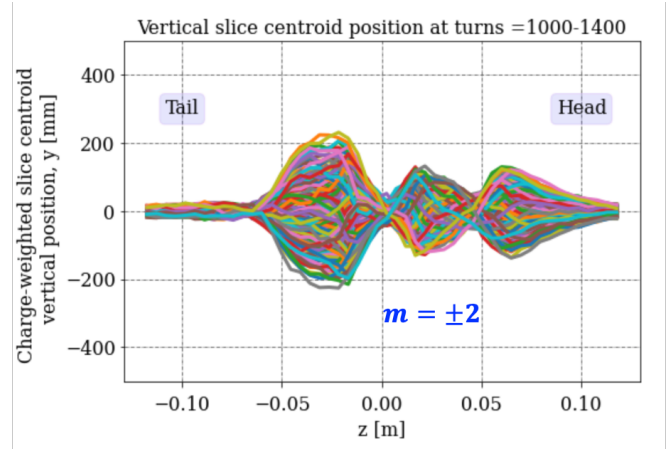


FIG. 20. Head tail instability result of the interaction of the beam with the electron cloud generated by the highest luminosity beam in the vacuum chamber of the HSR arc dipoles with SEY = 1.2.

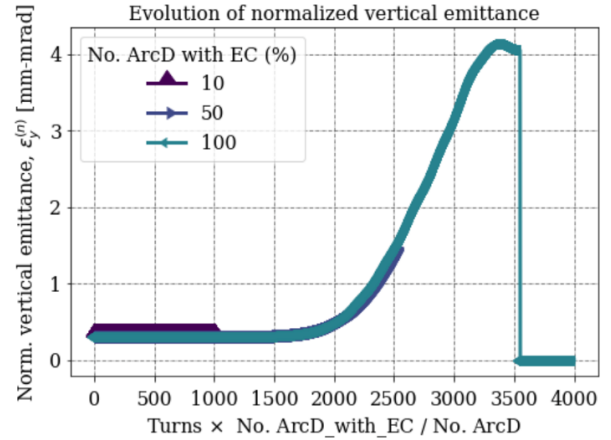


FIG. 21. Comparison of the evolution of normalized transverse emittance comparison in function of the number of arc dipoles that present electron cloud. The evaluation assumes electron density of $1e12$ e-/m³ (SEY ~ 1.08).

cloud led emittance growth even if the SEY is as low as 1.1 in every screen of an HSR arc dipole. The heat deposited by the electron cloud is pretty much proportional to the electron density, as seen from Fig. 4. The sharp logarithmic slope indicates an abrupt increase of electron density and deposited heat. Some slight difference on the onset of this slope arises from the non-uniform electron energy distribution. The stability study finds that the threshold for beam stability coincides with the threshold established from electron density to limit deposited heat.

V. POSSIBLE MITIGATIONS

Electron cloud buildup mitigations can be divided in active and passive methods [35]. Active methods include

the use of weak solenoid fields (10 – 20 G) along the vacuum chamber, biased clearing electrodes, selected bunch patterns, and beam ‘scrubbing’. Passive methods rely on the use of low SEY materials and coatings, grooved and LASE surfaces, specially shaped vacuum chambers, and vacuum procedures to reduce residual gas by in-situ baking and pre-pumping of cryogenic regions.

Electron cloud effect mitigations include Landau damping to control the head-tail transverse instability and the use of transverse bunch-by-bunch dampers.

A. Beam ‘scrubbing’

The SEY of a surface conditions with dose by several processes which include the removal of adsorbates (contaminants, adsorbed gases, etc.) and the modification of crystalline structure as it is the case with the carbon film’s graphitization [36]. A literature search found that typical doses to reduce the SEY of an amorphous carbon film from 1.3 to 1.0 are in the order of few mC/mm^2 to few tens of mC/mm^2 [37? ? , 38] for an electron energy comparable to that at which the SEY value reaches its maximum, around 300 eV for amorphous carbon. Typically the removal of contaminants requires less dose than the conversion of sp3 to sp2 bonds.

Beam ‘scrubbing’ consists on the generation of an electron cloud strong enough to induce dose conditioning in practical times while ensuring that the undesired effects of the electron cloud (deposited heat, beam stability) are kept under acceptable levels. Fig. ?? shows that for SEY values up to 1.2, the electron cloud generated by the highest luminosity beam drives emittance growth, thus preventing the delivery of the intended luminosity (luminosity is inversely proportional to beam emittance); however, the beam survives over many turns, opening its potential use for ‘scrubbing’ assuming that we start with a $\text{SEY} = 1.2$ surface for the beam screens at every HSR arc dipole. Although the goal is to produce amorphous carbon coatings with SEY close to 1, and store in N_2 back filled atmosphere while the beam screens await to be installed, exposure to air during installation may increase SEY. RHIC is warmed up every year but kept in vacuum; similar approach will be followed by the HSR. Occasional venting of some regions for installations, repairs, or maintenance may also increase SEY.

Scrubbing is most efficient by electrons with energies around 300 – 1000 eV. Fig. 22 shows that unfortunately most of the electrons in the electron clouds generated by the highest luminosity beam have impact energies below 100 eV. In addition, as the surface gets scrubbed and the SEY decreases, the electron cloud will become weaker, and in turn, the deposited dose will be smaller, reducing the efficiency of the conditioning as the ‘scrubbing’ process progresses. Under both considerations, Fig. ?? provides an estimate of the time required for the electron cloud to provide a total dose of $32 \text{ mC}/\text{mm}^2$ that conditions the surface of the beam screens in the HSR

arc dipoles from an initial SEY value of 1.2 down to 1.0. The different colored lines represent the estimated time to condition the surface to a particular SEY value. The estimate considers that electrons with energy above the threshold contribute equally to the conditioning of the surface whereas electrons with energy below the threshold do not contribute at all. Higher energy thresholds result in higher conditioning times because there are less electrons contributing to the conditioning, with the conditioning time estimate ranging from a few days to several weeks depending on the energy threshold.

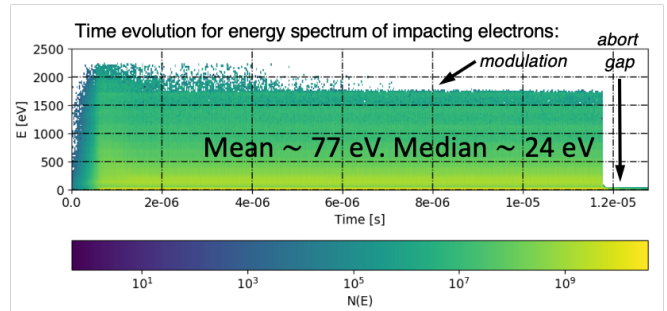


FIG. 22. Time evolution of the electron energy distribution over one turn.

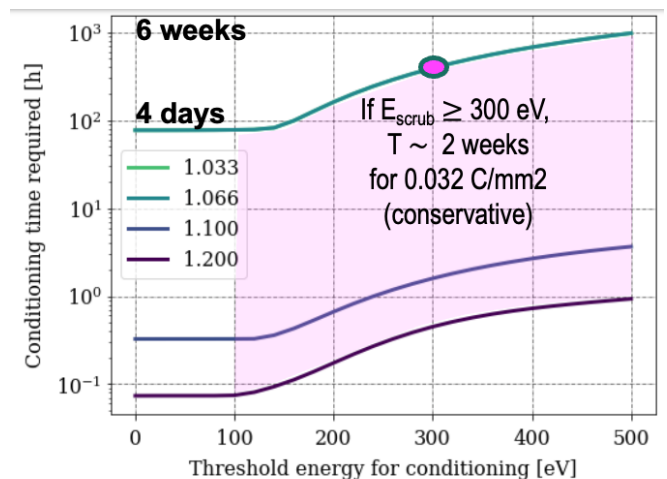


FIG. 23. Estimated conditioning time in function of the threshold energy.

The ‘scrubbing’ times required to condition the HSR vacuum chambers and prepare them to host the highest luminosity beam might differ from predictions because the dose delivered by the electron cloud is not uniform, and depends on the beam offset and the magnetic field pattern. The presented estimate assumes that the delivered dose is uniformly distributed across 2π , what may overestimate the time required to condition the surface. On the other hand, the collision mode requires the hadron beams to travel with a horizontal offset as large as 20 mm. Since the impact surfaces depend on the beam

offset, scrubbing needs to be performed for different beam offsets.

Some heat load budget is required for scrubbing. Nature sometimes helps and the heat deposited by electron clouds is larger for the highest luminosity beam than for the higher center-of-mass beam, whereas the heat from resistive wall is the opposite. In addition, the available heat load budget is contributed by all the cryomodules in a cooling circuit and not all will receive the same heat.

B. Landau damping

Octupoles introduce an amplitude-dependent tune shift which is proportional to the anharmonicity coefficients α_{ij} . For the HSR 275 GeV store optics, the maximum available α is about $2 \times 10^4 \text{ m}^{-1}$ with some caveats [39]. As emittance is the average amplitude of all particles in a bunch, $\varepsilon = \langle J_i \rangle_N$, the maximum detuning by HSR octupoles to 275 GeV proton beam with design normalized emittance is about 1×10^{-4} . In comparison, the tune spread experienced by the beam as a result of its interaction with the electron cloud is in the order of 1×10^{-2} , about two orders of magnitude larger than what the Landau octupoles can provide (see Fig. 24). While the Landau damping cannot correct the dQ introduced by the electron cloud, the HSR octupoles might still be handy to mitigate head-tail motion for other beams.

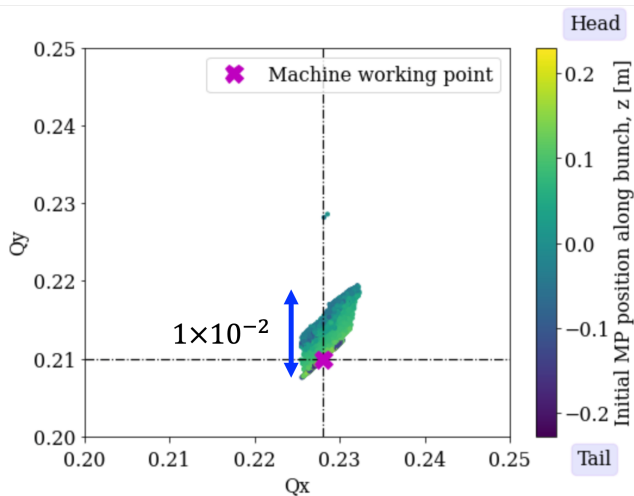


FIG. 24. Tune footprint of beam resulting from its interaction with the electron cloud. Octupoles are off.

VI. CONCLUSION AND OVERVIEW

Electron cloud buildup thresholds for many HSR beamline sections were estimated. The design of the components includes passive solutions to suppress e-cloud. Mitigation methods are being investigated such as ‘scrubbing’ to suppress electron cloud and Landau damping to ‘tame’ the associated head-tail oscillations. Further studies to determine electron cloud thresholds for other locations continue.

ACKNOWLEDGMENTS

The authors would like to thank Gianni Iadarola and Dean Hidas for technical support to run the simulations, Scott Berg for providing lattice parameters and magnet strengths, Charles Hetzel for providing the beam screen design, Frederic Micolon and Pete Braunius for information about the BPM design, Steve Peggs and Guillaume Robert-Demolaize for information on the beam offset, Roberto Than and Brian Gallagher for information on the heat load budget, and Xiaofeng Gu, Mike Blaskiewicz and Vadim Ptitsyn for valuable discussions about electron cloud and feedback on the studies reported on this paper.

MAGNET STRENGTHS AND TWISS PARAMETERS

Magnet strengths and Twiss parameters of the most recent lattice EIC-HSR-220921a for the 275 GeV proton beams in store (on-axis) are listed in Table V. The lattice for beams in collision is under preparation.

-
- [1] O. Malyshev and V. Baglin, in *Vacuum in Particle Accelerators*, Chap. 8.
 - [2] M. Blaskiewicz, Electron Cloud Effects in Present and Future High Intensity Hadron Machines, in *PAC 2003* (2003).
 - [3] G.I. Budker, G.I. Dimov, V.G. Dudnikov, Proceedings of the International Symposium on Electron and Positron Storage Rings, VIII-6-1, Saclay 1966.
 - [4] G.I. Budker, G.I. Dimov, V.G. Dudnikov, A.A. Sokolov, V.G. Shamovsky, Sixth International Conference on High Energy Accelerators, A-103, Cambridge Massachusetts,

TABLE V. Magnet strengths and Twiss parameters of lattice EIC-HSR-220921a for 275 GeV proton beams in store (on-axis).

Parameter	Arc D	Arc QF	Arc SF	Arc D	Arc QD	Arc SD
Strength (T/m ⁿ)	-3.782	-72.522	-368.877	-3.782	+74.275	+577.077
Order n	0	1	2	0	1	2
Length (m)	9.44	1.11	0.75	9.44	1.11	0.75
β_x (m)	39.72	11.48	11.63	14.38	48.20	47.65
β_y (m)	13.66	47.24	46.69	38.74	10.90	11.04
D_x (m)	1.1084	1.8951	1.8841	1.7172	1.0126	1.0185

- 1967.
- [5] V. Dudnikov, 8th ICFA Beam Dynamics Mini-workshop, Santa Fe, (2000), available online at <http://www.aps.anl.gov/conferences/icfa/two-stream.html>.
- [6] D. Neuffer, E. Colton, D. Fitzgerald, T. Hardek, R. Hutson, R. Macek, M. Plum, H. Thiessen, T.S. Wang NIM A321 p1 (1992).
- [7] M. A. Plum, D.H. Fitzgerald, D. Johnson, J. Langenbrunner, R.J. Macek, F. Merril, P. Morton, B. Prichard, O. Sander, M. Shulze, H.A. Thiessen, T.S. Wang, C.A. Wilkinson, PAC97 p 1611.
- [8] R. Macek, AIP Conf. 448, p116, (1998).
- [9] E. C. Raka, The Nature Of The Transverse Instability In The Brookhaven AGS, in *6th International Conference on High-Energy Accelerators* (1967) pp. 428–430, <https://inspirehep.net/files/60621ba177c461e4e9db5f473625b987>.
- [10] R. Cappi, M. Giovannozzi, E. Métral, G. Métral, G. Rumolo, and F. Zimmermann, Electron cloud buildup and related instability in the CERN Proton Synchrotron, Phys. Rev. ST Accel. Beams **5**, 094401 (2002).
- [11] G. Rumolo, H. Bartosik, E. Belli, G. Iadarola, K. Li, L. Mether, A. Romano, and M. Schenk, Electron cloud in the CERN accelerator complex, in *57th ICFA Advanced Beam Dynamics Workshop on High-Intensity and High-Brightness Hadron Beams* (2016) p. TUAM4X01.
- [12] G. Arduini, K. Cornelis, O. Grobner, N. Hilleret, W. Hofle, J. M. Jimenez, J. M. Laurent, G. Moulard, M. Pivi, and K. Weiss, Electron cloud: Observations with LHC-type beams in the SPS, in *7th European Particle Accelerator Conference (EPAC 2000)* (2000) pp. 939–941, <https://accelconf.web.cern.ch/e00/papers/THP1B16.pdf>.
- [13] J. Wenninger, LHC commissioning and first operation at 6.5 TeV, Congrès Général SFP 2015 - Strasbourg: https://indico.ijslab.in2p3.fr/event/2956/contributions/6669/attachments/6224/7368/LHC.SFP.Aout15_JorgWenninger_v2_talk1.pdf.
- [14] K. Li, H. Bartosik, G. Iadarola, L. Mether, A. Romano, G. Rumolo, and M. Schenk, Electron Cloud Observations during LHC Operation with 25 ns Beams, , TUPMW017 (2016).
- [15] S. Antipov, *Fast Transverse Beam Instability Caused by Electron Cloud Trapped in Combined Function Magnets*, Ph.D. thesis, Springer Theses. Springer, Cham. https://doi.org/10.1007/978-3-030-02408-6_1 (2017).
- [16] <https://accelconf.web.cern.ch/ipac2021/papers/tuxa03.pdf>.
- [17] <https://accelconf.web.cern.ch/e02/PAPERS/WEPRI034.pdf>.
- [18] Electron cloud measurements and simulations for the brookhaven relativistic heavy ion collider, ().
- [19] Electron cloud buildup driving spontaneous vertical instabilities of stored beams in the large hadron collider, ().
- [20] M. Blaskiewicz et al., The fast loss electron proton instability”, proc. workshop on instabilities of high intensity hadron beams in rings, <https://doi.org/10.1063/1.1303089>.
- [21] W. Fischer, J. M. Brennan, M. Blaskiewicz, and T. Sato-gata, Electron cloud measurements and simulations for the brookhaven relativistic heavy ion collider, Phys. Rev. ST Accel. Beams **5**, 124401 (2002).
- [22] W. Fisher et al., Electron cloud experiments and cures in rhic, https://accelconf.web.cern.ch/p07/TALKS/TUXABO2_TALK.PDF.
- [23] Y. Ji, *Electron Cloud Studies at Fermilab*, Ph.D. thesis (2018).
- [24] G. Iadarola, E. Belli, P. Dijkstal, L. Mether, A. Romano, G. Rumolo and E. Wulff, PyE-CLOUD Reference Manual (CERN, 2021) <https://raw.githubusercontent.com/PyCOMPLETE/PyE-CLOUD/master/doc/reference/reference.pdf>.
- [25] G. Iadarola, *Electron cloud studies for CERN particle accelerators and simulation code development*, PhD dissertation, Università degli Studi di Napoli Federico II, Dipartimento di Ingegneria Elettrica e Tecnologie dell’Informazione (DIETI), Napoli, Italy (2014), https://cds.cern.ch/record/1705520/files/CERN-THESIS-2014-047_2.pdf.
- [26] G. B. R. Salemme, V. Baglin and P. Chiggiato, Vacuum performance of amorphous carbon coating at cryogenic temperature with presence of proton beams (2016), proc. of IPAC’16, Busan, Korea, May 8-13, 2016 (JaCoW): 10.18429/JACoW-IPAC2016-THPMY007.
- [27] X. Gu, M. Blaskiewicz, A. Blednykh, G. Roberto-Demolaize, and S. Verdu-Andres, Electron Cloud Simulations for the Electron-Ion Collider in Brookhaven National Laboratory, EIC-ADD-TN-053; BNL-224221-2023-TECH (BNL, 2022) <https://doi.org/10.2172/1969916>.
- [28] F. Willeke and et al., *Electron Ion Collider Conceptual Design Report*, Tech. Rep. (Brookhaven National Laboratory, 2021).
- [29] S. Verdú-Andrés, *Electron cloud thresholds at the arcs of the Electron-Ion Collider hadron storage ring*, Tech. Rep. (BNL, 2023) <https://doi.org/10.2172/1992863>.
- [30] M. Van Gompel et al., Amorphous carbon thin film coating of the sps beamline: Evaluation of the first coating implementation, <https://inspirehep.net/literature/1626186>.
- [31] W. Vollenberg et al., Amorphous carbon coating in sps, <https://cds.cern.ch/record/2809481/files/document.pdf>.

- [32] C. Yin-Vallgren, *Low Secondary Electron Yield Carbon Coatings for Electron Cloud Mitigation in Modern Particle Accelerators*, PhD Dissertation, CERN-THESIS-2011-063, Department of Fundamental Physics Chalmers University of Technology Göteborg, Sweden 2011 (2011), <https://cds.cern.ch/record/1374938?ln=en>.
- [33] S. Berg, private communication on Nov. 23, 2022.
- [34] PyHEADTAIL github repository: ().
- [35] O. Malyshev and R. Valizadeh, Laser treatment at STFC, at the FCC-hh Impedance Beam-Screen Workshop (March 2017).
- [36] R. Larciprete, D. R. Grosso, A. Di Trollo, and R. Cimino, Evolution of the secondary electron emission during the graphitization of thin c films, *Applied Surface Science* **328**, 356 (2015).
- [37] M. Haubner, *Electron conditioning of technical surfaces at cryogenic and room temperature in the 0–1 keV energy range*, Ph.D. thesis, University of Geneva (2023), ph.D. thesis.
- [38] S. Bilgen, English *Dynamic pressure in particle accelerators: experimental measurements and simulation for the LHC*, Ph.D. thesis, Université Paris-Saclay (2020), ph.D. thesis.
- [39] S. Peggs, H. L. III, G. Robert-Demolaize, and A. Drees, *Resonance Island Jump Theory for the HSR*, Tech. Rep. EIC-ADD-TN-077 (Brookhaven National Laboratory, Upton, NY, USA, 2023) also available at <https://inspirehep.net/files/6a06fec924485b2c810199ce99e4fd27>.